DALTON
FULL PAPER

A new bis(μ-alkoxo) diiron(III) complex and its implications regarding the number of Fe(III)–phenolate bonds and the redox potential in uteroferrin

Ademir Neves,*[a] Liane M. Rossi,*[a] Ivo Vencato,[a] Wolfgang Haase[b] and Rüdiger Werner[b]

[a] *Departamento de Química, Universidade Federal de Santa Catarina, 88040-900 Florianópolis, SC, Brazil. E-mail: ademir@qmc.ufsc.br*
[b] *Institut für Physikalische Chemie, Technische Universität Darmstadt, D-64287 Darmstadt, Germany*

Received 7th October 1999, Accepted 12th January 2000

The first diiron(III) complex of the ligand *N*,*N*′-bis(2-hydroxybenzyl)-2-hydroxypropane-1,3-diamine (H_3bbpnol), $[Fe_2(bbpnol)_2]\cdot 2H_2O$ **1**, was prepared and fully characterized in order to model diiron metalloenzymes. The X-ray crystal structure determination together with the electrochemical data of **1** gave us sufficient information to infer the number of phenolates terminally bonded to the iron(III) centers in the active sites of Purple Acid Phosphatases (PAPs). Each iron(III) center in complex **1** has two O-phenolate atoms terminally coordinated. By comparison of redox potentials for the process $Fe^{III}{}_2$–$Fe^{III}Fe^{II}$ of the diiron PAP uteroferrin, complex **1** and complexes containing one, two and no phenolate oxygen atoms terminally bonded to the iron(III) centers, we confirmed the presence of only one terminal tyrosine group coordinated to the non-reducible iron(III) center, in agreement with the proposed structure of such metalloenzymes. The mixed-valence $Fe^{II}Fe^{III}$ derivative of **1** has been characterized by spectroelectrochemistry in the UV–VIS region. The $E^{\circ\prime}$ value obtained from the Nernst plot is in good agreement with CV data, and solutions of the $Fe^{II}Fe^{III}$ species are stable under argon on the time scale of the spectropotentiostatic experiment. Magnetic susceptibility measurements in the range 4.5 to 300 K indicate very weak antiferromagnetic coupling between the iron ions with $J = -2.2$ cm^{-1}, consistent with the long Fe–O distance and the small Fe–O–Fe angle within the bis(μ-alkoxo)diiron(III) entity.

Introduction

Purple acid phosphatases (PAPs) contain a dinuclear metal center in their active site and catalyze the hydrolysis of phosphoric acid esters under acidic conditions.[1,2] Of special interest in this respect are the mammalian enzymes, first identified in the bovine spleen (bsPAP) and porcine uterine fluids (uteroferrin, Uf). The active site of these enzymes contains a homonuclear diiron center with two accessible oxidation states: a reduced pink (λ_{max} = 505–510 nm, ε = 4000 dm^3 mol^{-1} cm^{-1}) $Fe^{II}Fe^{III}$ form and enzymatically active and a purple (λ_{max} = 550–570 nm, ε = 4000 dm^3 mol^{-1} cm^{-1}) oxidized $Fe^{III}Fe^{III}$ form which is inactive.[3,4] These bands are assigned as being tyrosinate to Fe^{III} transitions.[4] Based on the abnormally high ε of 4000 dm^3 mol^{-1} cm^{-1} compared to values of 1000 to 2000 per Fe^{III}–phenolate found for model complexes,[5] two tyrosine residues coordinated to the Fe^{III} center have been suggested.[6] However, no evidence of tyrosine heterogeneity has been found in the laser-Raman studies.[4,6] Moreover, absolute integration of the NMR signals relative to an internal standard[7] and larger ε_M values found in synthetic iron–phenolate complexes,[8] support the presence of only one tyrosine coordinated to the Fe^{III} center. The recent X-ray crystal structure determination of the related kidney bean PAP,[9] a heterodinuclear $Fe^{III}Zn^{II}$ enzyme, reveals the presence of one tyrosine (Tyr 167) coordinated to the ferric ion. On the basis of proton NMR studies on Zn-exchanged $Fe^{III}Fe^{II}$ kidney bean PAP and comparisons with the data of mammalian PAPs, a similar coordination environment around the dimetal active site of plant and mammalian PAPs has been proposed.[10] The presence of terminal histidine residues coordinated at each metal site has been demonstrated by NMR spectroscopy.[6b,7]

Temperature-dependent magnetic susceptibility measurements on the reduced and oxidized mammalian PAPs revealed that the iron centers are weakly antiferromagnetically spin coupled. Typical J values for the pink form are in the range −5 to −15 cm^{-1} and are characteristic of Fe^{II}(μ-OH)Fe^{III} systems.[2b] A recent magnetic susceptibility study of the oxidized bsPAP reveals that the coupling constant J lies in the range $-6 < J < -15$ cm^{-1}, which indicates the lack of a μ-oxo bridge.[11] On the other hand, these data are consistent with the presence of a μ-hydroxo bridge as observed in a great number of diiron model complexes.[2] Electrochemical studies using coulometric techniques show that the redox potentials for uteroferrin are 0.367 V at pH = 5.0 and 0.306 V at pH = 6.0 *vs.* NHE, which also indicates a μ-OH bridging unit.[12] Here, we report the synthesis, crystal structure, and some properties of the new dinuclear $[Fe^{III}{}_2(bbpnol)_2]\cdot 2H_2O$ **1** complex, (H_3bbpnol = *N*,*N*′-bis(2-hydroxybenzyl)-2-hydroxypropane-1,3-diamine),[13] which contains the Fe^{III}(μ-alkoxo)$_2Fe^{III}$ core and two phenolates coordinated at each Fe^{III} center. Besides the dinuclear Fe^{III}–$O_{phenolate}$ complexes already described in the literature,[13–20] complex **1** represents an additional interesting model which allowed us to correlate the number of terminal coordinated phenolate groups and the redox properties of such complexes and uteroferrin.

Experimental

Materials

Salicylaldehyde, 2-hydroxypropane-1,3-diamine, tetrabutylammonium hexafluorophosphate and iron(III) perchlorate were obtained from Aldrich Chemical Co. The reagents and solvents used in syntheses were reagent grade and used without further purification. Spectroscopic grade solvents from Merck were dried with molecular sieves for characterisation of the complex.

Syntheses

H_3bbpnol. This compound was prepared by the reaction between 2-hydroxypropane-1,3-diamine and salicylaldehyde followed by reduction with $NaBH_4$ according to the literature procedure.[13]

$[Fe_2(bbpnol)_2]\cdot 2H_2O$ 1. A 20 cm^3 methanol solution of H_3-bbpnol (0.302 g, 1 mmol) was added to a 20 cm^3 methanol solution of $Fe(ClO_4)_3\cdot xH_2O$ (0.354 g, 1 mmol) with stirring. Et_3N (0.7 cm^3, 5 mmol) was added slowly to the reaction mixture. After a few minutes of stirring and heating, precipitation could be observed. Following the workup procedure of filtration, washing with propan-2-ol–diethyl ether and drying, a brick-red product was obtained (0.17 g, 46%) (Found: C, 54.19; H, 5.32; N, 7.45. $Fe_2(bbpnol)_2\cdot 2H_2O$ ($Fe_2C_{34}H_{42}N_4O_8$) requires C, 54.71; H, 5.67; N, 7.51%); molar conductivity = 15 Ω^{-1} cm^2 mol^{-1}; IR bands/cm^{-1}: ν(OH) 3412s; ν(NH) 3274vs; ν(C=N, C=C) 1594s, 1480vs, 1452s; ν(CO) 1272vs; δ(CH Arom.) 762s. Single crystals suitable for X-ray structural analysis were obtained by recrystallisation from a methanol–dichloromethane complex solution.

Physical measurements

Elemental analysis results were obtained on a Perkin-Elmer 2400 instrument. The solution electrical conductivity was measured with a Digimed conductivity bridge, type CD-21, in acetonitrile solution at *ca.* 10^{-3} mol dm^{-3} at 25 °C. IR spectra were measured in the range 4000–400 cm^{-1} on a Perkin-Elmer model 781 spectrometer, on KBr pellets. Electronic absorption spectra in the range 200–1100 nm were recorded on a Perkin-Elmer Lambda-19 spectrophotometer. Magnetic susceptibility measurements were performed on a powder sample of the complex over the temperature range 4.5–300 K with a Faraday-type magnetometer. Details of the apparatus have been described elsewhere.[21] Diamagnetic corrections were applied in the usual manner with the use of tabulated Pascal constants.[22] Electrochemical measurements were carried out using a Princeton Applied Research (PARC) model 273 potentiostat/galvanostat. Cyclic voltammetry measurements were obtained at room temperature for acetonitrile solutions containing *ca.* 10^{-3} mol dm^{-3} complex and 0.1 mol dm^{-3} $[NBu^n_4][PF_6]$ as the supporting electrolyte under an argon atmosphere. The electrochemical cell employed was of a standard three-electrode configuration: a glassy carbon working electrode (3 mm diameter), a platinum wire counter electrode, and a SCE reference electrode constructed in our laboratory. The Fc^+–Fc couple of ferrocene (E° = 0.400 V *vs.* NHE) was used as an internal standard.[23] The $E_{1/2}$ of ferrocene was 0.157 V *vs.* SCE. Spectroelectrochemical experiments were performed using an optically transparent thin-layer cell on a Perkin-Elmer Lambda-19 spectrophotometer and the potentials being applied to the cell by a PARC model 263 potentiostat/ galvanostat. The optically transparent thin-layer cell was constructed as follows: the transparent electrode was a 500 wires per inch (60% transmittance) Buckbee Mears Co. gold minigrid, sandwiched between two microscope slides by a Teflon tape spacer. The minigrid acts as a working electrode and extended outside of the slides for electrical contacts. A platinum wire counter electrode and a SCE reference electrode complete the three-electrode configuration. The performance of the reference electrode was monitored before and after the experiments, by measuring the Fc^+–Fc couple of ferrocene ($E_{1/2}$ = 0.530 V *vs.* SCE). The measurements were carried out at room temperature for an acetonitrile solution degassed under an argon atmosphere, containing >10^{-3} mol dm^{-3} complex and 0.1 mol dm^{-3} $[NBu^n_4][PF_6]$ as the supporting electrolyte.

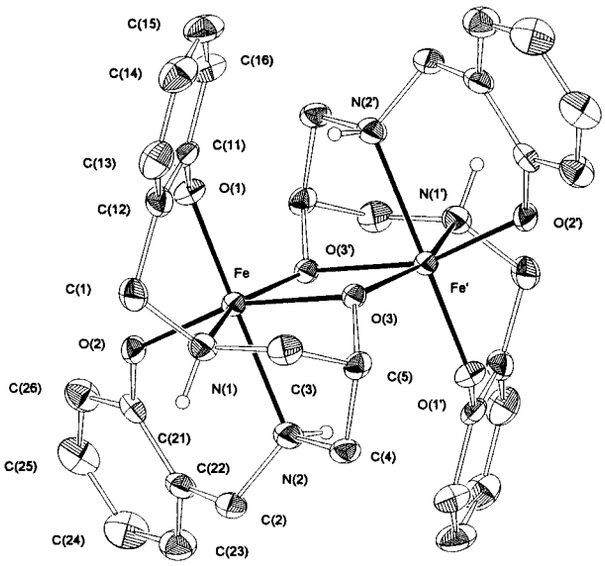

Fig. 1 A ZORTEP view of the neutral complex $[Fe_2(bbpnol)_2]$, showing the atom labeling scheme at 30% probability level. Hydrogen atoms have been omitted for clarity except those on the amino groups, which are represented as spheres of arbitrary size.

Crystal structure determination of complex 1

Crystal Data. $C_{34}H_{38}Fe_2N_4O_6\cdot 2H_2O$ **1**, M = 746.42, triclinic, a = 9.653(2), b = 9.754(2), c = 9.848(2) Å, α = 89.02(3), β = 80.92(3), γ = 66.11(3)°, U = 836.1(3) $Å^3$, T = 293 K, space group $P\bar{1}$ (no. 2), Z = 1, μ(Mo-Kα) = 0.925 mm^{-1}, D_c = 1.483 Mg m^{-3}, 3131 reflections measured, 2939 unique, (R_{int} = 0.0425) which were used in all calculations. The final $wR(F^2)$ was 0.1128 (all data) for 224 refined parameters.[24–26]

CCDC reference number 186/1799.

See http://www.rsc.org/suppdata/dt/a9/a908062g for crystallographic files in .cif format.

Results and discussion

Syntheses

The ligand $bbpnol^{3-}$ is a potentially dinucleating ligand and provides two N-amine, two O-phenolates and an O-alkoxide as donor groups.

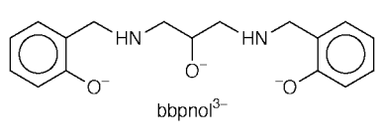

$bbpnol^{3-}$

In the presence of Et_3N, the ligand H_3bbpnol reacts in methanol with iron(III) perchlorate in a 1:1 stoichiometry to form a stable neutral dinuclear complex: $[Fe_2(bbpnol)_2]\cdot 2H_2O$ **1**. The neutral behaviour of the complex is confirmed by the low molar conductivity (15 Ω^{-1} cm^2 mol^{-1}) characteristic of neutral species.[27]

Crystal structure of $[Fe_2(bbpnol)_2]\cdot 2H_2O$ 1

A ZORTEP[28] view of the centrosymmetric complex is shown in Fig. 1. Selected bond distances and angles are listed in Table 1. The structure shows a dimeric unit where each Fe^{III} ion takes a distorted octahedral geometry and the alkoxide group of both ligands provides the two bridging atoms for the dimeric unit, forming a $Fe_2(OR)_2$ core. The center of symmetry lies in the center of this core. Each Fe^{III} atom is coordinated by the pentadentate ligand which is completely deprotonated. The

ligand is coordinated in such a way that one phenolate oxygen atom and one amine nitrogen atom are *trans* in axial positions, and the other phenolate oxygen atom and amine nitrogen atom groups are *cis*, defining the equatorial plane with the two alkoxo oxygen bridging atoms. All bond distances are in the range observed in other Fe^{III}–O,N donor ligand complexes containing related ligands $[FeL(OH)]_2 \cdot 2H_2O \cdot 2py$ (L = *N*,*N*′-ethylenebis(salicylamine))[29] and $[Fe_2(L)_2] \cdot 2MeCN$ (H_3L = 1-salicylideneamino-3-salicylaminopropan-2-ol).[30] The chelating system produces two five-membered and two six-membered metallacycles at each iron center. The presence of five-membered rings between O(3), N(1) and O(3), N(2) leads to a decrease from the ideal value of 90° for the angle O(3)–Fe–N(1) [79.7(1)°] and O(3)–Fe–N(2) [74.3(1)°]. It results in distortions in the remaining angles in the coordination sphere from ideal octahedral symmetry. The $FeNO_3$ (equatorial plane) group varies somewhat from planarity (0.10 Å). Steric requirements for the ligand produce variations from 90° for equatorial–axial bond angles {O–Fe–N angles [74.3(1)°, 86.8(1)°, 88.8(1)°], O–Fe–O angles [99.8(1)°, 99.2(1)°, 98.7(1)°] and N–Fe–N angles [81.4(2)°]}, and a distortion from 180° for the O(1)–Fe–N(2) (axial–axial) bond angle [169.1(2)°]. The iron is 0.23(1) Å out of this plane. The Fe–O_{alkoxo} bond distances [1.985(3) and 2.063(3) Å] are inequivalent. This difference has been observed in other similar bis(μ-alkoxo) complexes.[30–35] The Fe–O–Fe–O ring is planar (360°). The Fe–O–Fe angle [101.1(1)°] is the smallest value found for bis(μ-alkoxo) complexes, whereas the Fe · · · Fe separation of 3.125 Å is in the mid-range. Table 2 shows structural data of related complexes for comparison. There is an intramolecular hydrogen bond N(2)–H(2) · · · O(1^i) with H(2) · · · O(1^i) 2.44 and N(2) · · · O(1^i) 3.147(6) Å and N(2)–H(2) · · · O(1^i) angle of 135.1°. The water molecule is hydrogen bonded to the O phenolate atoms of different complex molecules [OW · · · O(1^i) 3.040(6) and OW · · · O(2^{ii}) 2.837(6) Å] with the symmetry codes: (i) = $-x + 1$, $-y + 1$, $-z + 2$; (ii) = $x - 1$, y, z.

Table 1 Selected bond distances (Å) and angles (°) for $[Fe_2(bbpnol)_2] \cdot 2H_2O$ **1** [a]

Fe–O(2)	1.905(3)	Fe–O(3)	2.063(3)
Fe–O(1)	1.916(3)	Fe–N(1)	2.184(4)
Fe–O(3′)	1.985(3)	Fe–N(2)	2.212(4)
O(2)–Fe–O(1)	98.69(14)	O(3′)–Fe–N(1)	158.20(14)
O(2)–Fe–O(3′)	101.99(14)	O(3)–Fe–N(1)	79.67(14)
O(1)–Fe–O(3′)	99.17(13)	O(2)–Fe–N(2)	86.82(14)
O(2)–Fe–O(3)	161.13(12)	O(1)–Fe–N(2)	169.10(15)
O(1)–Fe–O(3)	99.75(13)	O(3′)–Fe–N(2)	88.78(14)
O(3′)–Fe–O(3)	78.94(13)	O(3)–Fe–N(2)	74.33(13)
O(2)–Fe–N(1)	96.88(15)	N(1)–Fe–N(2)	81.40(16)
O(1)–Fe–N(1)	88.57(14)		

[a] Primed atoms are generated by the symmetry operation $-x + 1$, $-y + 1$, $-z + 2$.

Magnetochemistry

Variable temperature magnetic data for $[Fe_2(bbpnol)_2] \cdot 2H_2O$ **1** in the range 4.5–300 K show that antiferromagnetic coupling exists (Fig. 2). The data were fitted by using eqn. (1)[41] for molar susceptibility *versus* temperature derived from the spin-exchange Hamiltonian $H = -2J(S_1S_2)$ with $S_1 = S_2 = 5/2$.

$$\chi(T) = (1 - x_p)\chi_{dim}(T) + 2x_p\chi_p(T) + 2N_\alpha \qquad (1)$$

with

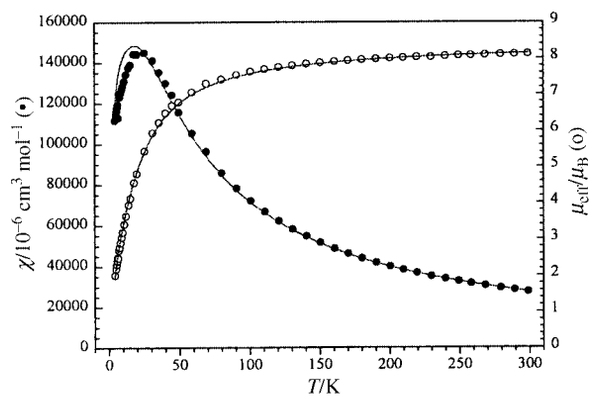

Fig. 2 Temperature dependence of the magnetic susceptibility of complex $[Fe_2(bbpnol)_2] \cdot 2H_2O$ **1**. The solid lines correspond to the best fit values.

Table 2 Structural and magnetic data for bis(μ-alkoxo)diiron(III) complexes

Complex	Fe · · · Fe/Å	Fe–O–Fe/°	P [a]/Å	J_{exp}/cm^{-1}	J_{calc} [b]/cm^{-1}	Ref.
$[Fe_2(L)_2]$ [c]	3.187	101.9	2.0515	−2.8 [d]	−4.6	30
$[Fe_2(salpa)_2(salph)_2]$ [e]	3.217	110.6–108.2	1.957	—	−15.2	31
$[Fe_2(dbe)_2(OBz)_2]^{2+}$ [f]	3.210	107.4	1.995	−20.5	−9.4	32
$[Fe(heidi)(H_2O)]_2$ [g]	3.119	104.3	1.9755	−13.4	−12.0	33
$[Fe\{(N(PL)_2)_2ala\}]_2^{2+}$ [h]	3.180	103.8	2.0205	−5.2	−6.8	34
$[Fe_2(OMe)_2(chp)_4(dmbipy)_2]$ [i]	3.194	104.7	2.016	−26.8	−7.2	35
$[Fe_2(OMe)_2(chp)_4(phen)_2]$ [j]	3.153	104.3	1.997	−28.6	−9.1	35
$[Fe_2(acac)_4(OEt)_2]$ [k]	3.116	103.6	1.982	−11.0	−11.0	36
$[Fe_2L(OEt)Cl_2]$ [l]	3.144	104.3	1.991	−15.4	−9.9	36
$[Fe_2L(OMe)Cl_2]$ [l]	3.106	103.0	1.995	−16.3	−9.4	37
$[Hpy]_2[Fe_2(cit)_2(H_2O)_2]$ [m]	3.120	—	2.0125	−4.5	−7.5	38
$[Fe_2(L)_2(OMe)_2]$ [n]	3.168	104.6	2.002	−10.9	−8.6	39
$[Fe_2(OEt)_2Cl_6]^{2-}$	3.117	107.0	1.9755	−24.6	−12.0	40
$[Fe(cupf)_2(OMe)]_2$ [o]	3.075	102.4	1.9725	−14.0	−12.5	41
$[Fe(salpa)Cl]_2$ [e]	3.089	104.1	1.955	−17.0	−15.6	42
$[Fe_2(bbpnol)_2]$	3.125	101.1	2.024	−2.2	−6.5	This work

[a] Half of the shortest super-exchange pathway between two iron(III) ions. [b] Calculated using the exponential relationship $-J = A\exp(BP)$ and the reported values $A = 8.763 \times 10^{11}$ and $B = -12.662$.[43] [c] H_3L = 1-Salicylideneamino-3-salicylaminopropan-2-ol. [d] The magnetic susceptibility data were collected in the temperature range 80–300 K. [e] H_2salpa = *N*-(3-Hydroxypropyl)salicylaldimine. [f] Hdbe = 2-[Bis(2-benzimidazolylmethyl)amino]-ethanol. [g] H_3heidi = [*N*,*N*′-Di(2-acetate)-*N*-2-(hydroxyethyl)]amine. [h] $H_2N(PL)_2$ala = α,3-Dihydroxy-β-{[(3-hydroxy-5-hydroxymethyl-2-methyl-4-pyridyl)methylene]amino}-5-hydroxymethyl-α,2-dimethyl-4-pyridylpropanoic acid. [i] Hchp = 6-Chloro-2-pyridone, dmbipy = 4,4′-dimethyl-2,2′-bipyridine. [j] phen = 1,10-Phenanthroline. [k] acac = Pentane-2,4-dionate. [l] H_3L = 1,4-Piperazinediyl-bis(*N*-ethylenesalicylaldimine). [m] py = Pyridine, H_4cit = citric acid. [n] H_2L = pimelyl-bis(*N*-isopropylhydroxamic acid). [o] Hcupf = PhN(OH)NO (cupferron).

$$\chi_{dim}(T) = (C/T) \times \frac{2\exp(2x) + 10\exp(6x) + 28\exp(12x) + 60\exp(20x) + 110\exp(30x)}{1 + 3\exp(2x) + 5\exp(6x) + 7\exp(12x) + 9\exp(20x) + 11\exp(30x)}$$

and $\chi_p(T) = (C/3T)S(S + 1)$; $C = N_A g^2 \mu_B^2/k$; $x = J/kT$ and $S = 5/2$.

For a satisfactory fit, the following parameters: $J = -2.2(3)$ cm^{-1}, $g = 2.00(1)$ (fixed),% impurity = 0.0, and TIP = 400 × 10^{-6} cm^3 mol^{-1} were used. The weak antiferromagnetic spin coupling constant of -2.2 cm^{-1} lies on the lower end of the range of values found for bis(μ-alkoxo)diiron(III) complexes shown in Table 2. In fact, the extent of antiferromagnetic interaction in such doubly bridged Fe^{III} dimers is very sensitive to the structural parameters of the bridges, *i.e.*, the Fe–O distances and Fe–O–Fe angles, as a consequence of the planarity or near-planarity of the Fe(OR)$_2$Fe bridging core. The quantitative magnetostructural relationship, $-J_{calc} = A\exp(BP)$, for dinuclear Fe^{III} centers bridged by a ligand oxygen atom (oxo, hydroxo, alkoxo, *etc.*) described by Gorun and Lippard,[43] correlates the antiferromagnetic super-exchange coupling J with a parameter P, describing half of the shortest super-exchange pathway between the two metal centers. An estimation of the magnitude of exchange interaction in [Fe$_2$(bbpnol)$_2$]·2H$_2$O **1** and related bis(μ-alkoxo)diiron(III) complexes, by using the reported A and B parameters[43] and P from X-ray structural data (Table 2), reveals that this correlation has only a limited validity for this type of complexes. The deviations between measured and calculated values of J are relatively large. The $-J_{calc} = 6.5$ cm^{-1} value obtained for complex **1** is approximately three times larger than that observed experimentally ($-J_{calc} = 2.2$ cm^{-1}). From this information, it seems reasonable to consider that for doubly bridged Fe^{III} complexes containing the Fe(OR)$_2$Fe bridging core, half of the shortest super-exchange pathway (P) is not the only determining factor as usually observed in oxo-bridged dimers.[43] On the other hand, all attempts to correlate the bridging Fe–O–Fe angle with the magnitude of J, based on the semi-empirical angular overlap model recently described by Weihe and Güdel,[44] were also unsuccessful for the complexes listed in Table 2. Moreover, a direct interaction between the Fe^{III} centers can be excluded for this type of complexes owing to the large metal-metal distance (>3 Å).[45] In general, J increases with an increased Fe–O–Fe angle in planar structures and with a decrease in the shortest super-exchange pathway, as already observed for other bis(μ-alkoxo)diiron(III) complexes.[35] Therefore, the smaller Fe–O–Fe angle in conjunction with the longer Fe–O distance in **1**, compared to other bis(μ-alkoxo) complexes listed in Table 2, may be responsible for the lower degree of antiferromagnetic coupling in **1**.

UV–VIS Spectroscopy

The electronic spectrum of [Fe$_2$(bbpnol)$_2$]·2H$_2$O **1** measured in acetonitrile reveals the following transitions at λ_{max}/nm (ε/dm^3 mol^{-1} cm^{-1}): 436 (4400), 312 (sh, 8000) and 277 (14800). Under an octahedral crystal field, high-spin Fe^{III} should show only very weak d–d transitions bands, because all transitions are spin forbidden. Thus the absorption bands at 436 nm and 312 nm may be assigned to phenolate–Fe^{III} charge transfer transitions (LMCT) from p_π orbitals to d_{π^*} and d_{σ^*}, respectively. The intense absorption in the higher energy region may be assigned to an intra-ligand transition.

Electrochemistry and spectroelectrochemistry

The cyclic voltammogram of [Fe$_2$(bbpnol)$_2$]·2H$_2$O **1** is illustrated in Fig. 3. The complex shows a *quasi*-reversible redox couple at -0.93 V *vs.* NHE corresponding to the Fe$^{III}_2$–Fe^{III}Fe^{II} couple. The quasi-reversible behaviour of the redox process is evident from the adherence to the following criteria: (i) the $E_{1/2}$ values ($E_{1/2} = 0.5(E_{pa} + E_{pc})$ are independent of scan rates

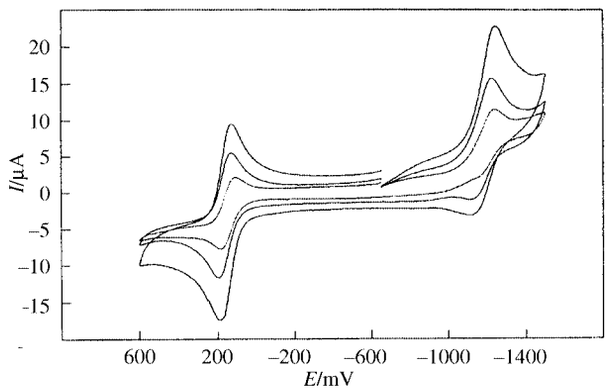

Fig. 3 Cyclic voltammogram of [Fe$_2$(bbpnol)$_2$]·2H$_2$O **1** in MeCN (0.1 mol dm^{-3} [NBu$^n_4$][PF$_6$] supporting electrolyte, glassy carbon working electrode (diameter 3 mm), ferrocene internal standard, scan rates of 50, 100 and 200 mV s^{-1}).

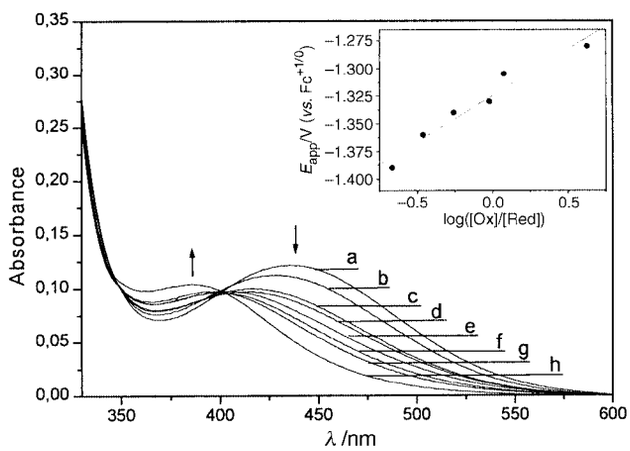

Fig. 4 Spectral changes during spectropotentiostatic experiments of [Fe$_2$(bbpnol)$_2$]·2H$_2$O **1** (0.1 mol dm^{-3} [NBu$^n_4$][PF$_6$] in MeCN). Applied potentials in V *vs.* Fc$^+$–Fc^0 are: (a) −0.530; (b) −1.280; (c) −1.305; (d) −1.330; (e) −1.340; (f) −1.360; (g) −1.390; (h) −1.530. The inset shows the Nernst plot.

(50 to 200 mV s^{-1}); (ii) $\Delta E_p > 60$ mV and increases with scan rate (100 mV at 50 mV s^{-1} to 126 mV at 200 mV s^{-1}); (iii) $I_{pa}/I_{pc} < 1$. The Fe^{III}Fe^{II} derivative of **1** should be electrochemically readily accessible while the Fe$^{II}_2$ form will be more difficult to obtain. A spectroelectrochemical study was performed under the same conditions as the CV experiments to explore the accessibility of the mixed valence Fe^{III}Fe^{II} derivative. Spectral changes in the range 320–600 nm, after equilibrium was established following selected potential steps, for the reaction of Fe$^{III}_2$ to Fe^{III}Fe^{II} are shown in Fig. 4. The maintenance of a isosbestic point in successive spectra indicates the presence of a single product throughout the course of the electrolysis. Data were analysed by means of the Nernst equation: $E_{app} = E^{\circ\prime} + (0.059/n)$ log [Ox]/[Red], where E_{app} = applied potential, $E^{\circ\prime}$ = standard potential, n = number of electrons transferred, $[Ox]/[Red] = (A_i - A_{red})/(A_{ox} - A_i)$ with A_{ox} = absorbance of the fully oxidized species, A_{red} = absorbance of the fully reduced species and A_i = absorbance at each potential after equilibrium was established. The Nernst plot, E_{app} *vs.* log[Ox]/[Red], should be a linear correlation with a linear coefficient of $E^{\circ\prime}$ and a slope of 0.059/n at 25 °C.[46] The $E^{\circ\prime} = -0.924 \pm 0.004$ V *vs.* NHE and $n = 0.80 \pm 0.1$ electron values obtained from the Nernst plot (inset of Fig. 4) using the absorbance recorded at 480 nm agree very well with the CV results. It is interesting that the band at 436 nm (Fe$^{III}_2$ species)

Table 3 Electrochemical data for the $Fe^{III}{}_2$–$Fe^{III}Fe^{II}$ process in diiron complexes[a]

Complex	Number of $Fe–O_{phenolate}$ terminal bonds	$E_{1/2}$[b]/V (*vs.* NHE)	Ref.
$[Fe_2(bbpnol)_2]$	4	−0.93	This work
$[Fe_2(bbppnol)(MeCO_2)_2]^{+}$ [c]	2	−0.21	13
$[Fe_2(bbpmp)(MeCO_2)_2]^{+}$ [d]	2	−0.17	14
$[Fe_2L(\mu\text{-}OMe)(OMe_2)]^{+}$ [e]	2	0.02	15
$[Fe_2(bpbpmp)(MeCO_2)_2]^{+}$ [f]	1	0.38	16
$[Fe_2(L\text{-}Bzim)(MeCO_2)_2]^{2+}$ [g]	0	0.57	17
$[Fe_2(tpdb)(PhCO_2)_2]^{+}$ [h]	0	0.625	18
$[Fe_2(bpmp)(OPr^n)_2]^{2+}$ [i]	0	0.67	19
$[Fe_2(L\text{-}py)(MeCO_2)_2]^{2+}$ [i]	0	0.69	20
$[Fe_2(bpmp)(PhCO_2)_2]^{2+}$ [i]	0	0.728	19
Uteroferrin (at pH = 6.0)	1	0.306	12
Uteroferrin (at pH = 5.0)	1	0.367	12

[a] Complexes for which the Fc^{+}–Fc couple has been used as internal standard. [b] Potentials were referred *vs.* NHE by adding 0.400 V to the potentials corrected *vs.* Fc^{+}–Fc.[23] [c] H_3bbppnol = *N*,*N*′-Bis(2-hydroxybenzyl)-*N*,*N*′-bis(2-pyridylmethyl)-2-hydroxypropane-1,3-diamine. [d] H_3bbpmp = 2,6-Bis[(2-hydroxybenzyl)(2-pyridylmethyl)aminomethyl]-4-methylphenol. [e] H_3L = 2-Bis[{(2-pyridylmethyl)aminomethyl}-6-bis-{(2-hydroxyphenyl)}aminomethyl]-4-methylphenol. [f] H_2bpbpmp = 2-Bis[{(2-pyridylmethyl)aminomethyl}-6-{(2-hydroxybenzyl)(2-pyridylmethyl)}aminomethyl]-4-methylphenol. [g] HL-Bzim = 2,6-Bis[bis-(2-benzimidazolylmethyl)aminomethyl]-4-methylphenol. [h] tpdb = *N*,*N*,*N*′,*N*′-Tetrakis(2-pyridylmethyl)-1,4-diaminobutan-2-olate. [i] HL-py or Hbpmp = 2,6-bis[bis(2-pyridylmethyl)aminomethyl]-4-methylphenol.

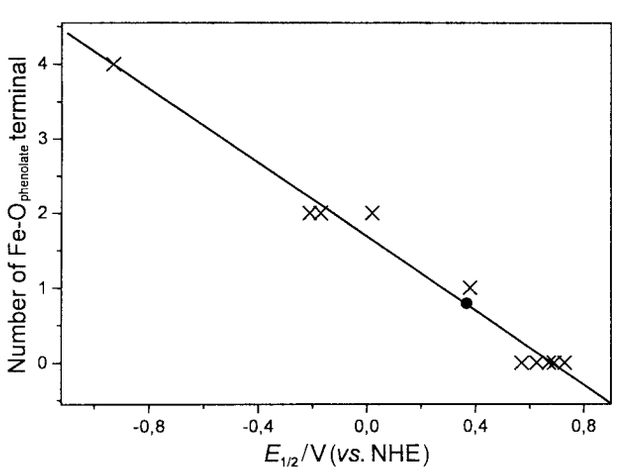

Fig. 5 Diagram correlating the number of $Fe^{III}–O_{phenolate}$ terminal bonds with the redox potential for the process $Fe^{III}{}_2$–$Fe^{III}Fe^{II}$ in the complexes of Table 3 (×) and in Uf (●).

moved to 385 nm ($Fe^{III}Fe^{II}$ species) without significant changes in the intensity of the absorption band. Moreover, these data confirm the accessibility of the mixed-valence $Fe^{II}Fe^{III}$ species in solution without changing the coordination sphere at the iron centers.

We found a linear correlation between the number of phenolates coordinated terminally to the Fe^{III} ions and the redox potential for the process $Fe^{III}{}_2Fe^{III}Fe^{II}$ upon comparison of the redox potential of $[Fe_2(bbpnol)_2]\cdot 2H_2O$ **1** and the corresponding values for a series of complexes containing different number of phenolate groups terminally coordinated to the two iron(III) centers, shown in Table 3. The $E^{\circ\prime}$ values for the diiron PAP uteroferrin (0.367 V *vs.* NHE at pH = 5.0 and 0.306 at pH = 6.0),[12] when fitted into this linear correlation, correspond to the value of one phenolate terminally bonded to the iron(III) centers.

In conclusion, this correlation strongly corroborates with the proposed structure of the diiron PAP,[4,6,7] in which only one tyrosine should be coordinated to the non-reducible Fe^{III} center. Finally, it is important to note that the linear trend found in Fig. 5 can be used in the design of multidentate ligands containing different numbers of phenolate groups for the stabilization of preferred oxidation states of diiron complexes.

Acknowledgements

This work was supported by grants from CNPq and PRONEX.

References

1 T. Klabunde and B. Krebs, *Struct. Bonding* (*Berlin*), 1997, **89**, 177; K. Doi, B. C. Antanaitis and P. Aisen, *Struct. Bonding* (*Berlin*), 1988, **70**, 1.
2 (*a*) J. B. Vincent, G. L. Olivier-Lilley and B. A. Averill, *Chem. Rev.*, 1990, **90**, 1447; (*b*) D. M. Kurtz, Jr., *Chem. Rev.*, 1990, **90**, 585.
3 H. D. Campbell, D. A. Dionysius, D. T. Keough, B. F. Wilson, J. de Jersey and B. Zerner, *Biochemistry*, 1978, **82**, 615.
4 B. C. Antanaitis and P. Aisen, *Adv. Inorg. Biochem.*, 1983, **5**, 111; B. C. Antanaitis, T. Strekos and P. Aisen, *J. Biol. Chem.*, 1982, **257**, 3766.
5 R. H. Heistand, R. B. Lauffer, E. Fikrig and L. Que, Jr., *J. Am. Chem. Soc.*, 1982, **104**, 2789; E. W. Ainscough, A. M. Brodie, J. E. Plowman, K. L. Brown, A. W. Addison and A. R. Gainsford, *Inorg. Chem.*, 1980, **19**, 3655.
6 (*a*) B. A. Averill, J. C. Davis, S. Burman, T. Zirino, J. Sanders-Loehr, T. M. Loehr, J. T. Sage and P. G. Debrunner, *J. Am. Chem. Soc.*, 1987, **109**, 3760; (*b*) R. B. Laufer, B. C. Antanaitis, P. Aisen and L. Que, Jr., *J. Biol. Chem.*, 1983, **258**, 14212.
7 R. C. Scarrow, J. W. Pyrz and L. Que, Jr., *J. Am. Chem. Soc.*, 1990, **112**, 657.
8 S. Yan, L. Que, Jr., L. F. Taylor and O. P. Anderson, *J. Am. Chem. Soc.*, 1988, **110**, 5222.
9 N. Sträter, T. Klabunde, P. Tucker, H. Witzel and B. Krebs, *Science*, 1995, **268**, 1489.
10 G. Battistuzzi, M. Dietrich, R. Löcke and H. Witzel, *Biochemistry*, 1997, **323**, 593.
11 S. Gehring, P. Fleischhauer, M. Behlendorf, M. Hüber, J. Lorösch, W. Haase, M. Dietrich, H. Witzel, R. Löcke and B. Krebs, *Inorg. Chim. Acta*, 1996, **252**, 13.
12 D. L. Wang, R. C. Holz, S. S. David, L. Que, Jr. and M. T. Stankovich, *Biochemistry*, 1991, **30**, 8187.
13 A. Neves, S. M. D. Erthal, V. Drago, K. Griesar and W. Haase, *Inorg. Chim. Acta*, 1992, **197**, 121.
14 A. Neves, M. A. de Brito, V. Drago, K. Griesar, W. Haase and Y. P. Mascarenhas, *Inorg. Chim. Acta*, 1993, **214**, 5.
15 C. Belle, I. Gautier-Luneau, J. L. Pierre and C. Scheer, *Inorg. Chem.*, 1996, **35**, 3706.
16 A. Neves, M. A. de Brito, V. Drago, K. Griesar and W. Haase, *Inorg. Chim. Acta*, 1995, **237**, 131.
17 M. Suzuki, H. Oshio, A. Uehara, K. Endo, M. Yanaga, S. Kida and K. Saito, *Bull. Chem. Soc. Jpn*, 1988, **61**, 3907.
18 M. Suzuki, S. Fujinami, T. Hibino, H. Hori, Y. Maeda, A. Uehara and M. Suzuki, *Inorg. Chim. Acta*, 1998, **283**, 124.
19 A. S. Borovik, V. Papaefthymiou, L. F. Taylor, O. P. Anderson and L. Que, Jr., *J. Am. Chem. Soc.*, 1989, **111**, 6183.
20 M. Suzuki, A. Uehara, H. Oshio, K. Endo, M. Yanaga, S. Kida and K. Saito, *Bull. Chem. Soc. Jpn.*, 1987, **60**, 3547.
21 L. Merz and W. Haase, *J. Chem. Soc.*, *Dalton Trans.*, 1980, 875.
22 C. J. O'Connor, *Prog. Inorg. Chem.*, 1982, **29**, 203.
23 R. R. Gagné, C. A. Koval and G. C. Lisensky, *Inorg. Chem.*, 1980, **19**, 2854.
24 C. K. Fair, MOLEN. An interative intelligent system for crystal structure analysis, Enraf-Nonius, Delft, 1990.
25 G. M. Sheldrick, SHELXS97: Program for the solution of crystal structures, University of Göttingen, Göttingen, 1997.
26 G. M. Sheldrick, SHELXL97: Program for the refinement of crystal structures, University of Göttingen, Göttingen, 1997.
27 W. J. Geary, *Coord. Chem. Rev.*, 1971, **7**, 81.
28 L. Zsolnai, ZORTEP: An interactive ORTEP program, University of Heidelberg, Heidelberg, 1996.
29 L. Borer, L. Thalken, C. Ceccarelli, M. Glick, J. H. Zhang and W. M. Reiff, *Inorg. Chem.*, 1983, **22**, 1719.
30 M. Mikuriya, Y. Yamato and T. Tokii, *Chem. Lett.*, 1992, 1571.
31 J. A. Bertrand and P. G. Eller, *Inorg. Chem*, 1974, **13**, 927.
32 S. Ménage and L. Que, Jr., *Inorg. Chem.*, 1990, **29**, 4293.

33 A. K. Powell, S. L. Heath, D. Gatteschi, L. Pardi, R. Sessoli, G. Spina, F. Del Giallo and F. Pieralli, *J. Am. Chem. Soc.*, 1995, **117**, 2491.
34 G. J. Long, J. T. Wrobleski, R. V. Thundathil, D. M. Sparlin and E. O. Schlemper, *J. Am. Chem. Soc.*, 1980, **102**, 6040.
35 A. J. Blake, C. M. Grant, S. Parsons, G. A. Solan and R. E. P. Winpenny, *J. Chem. Soc.*, *Dalton Trans.*, 1996, 321.
36 B. Chiari, O. Piovesana, T. Tarantelli and P. F. Zanazzi, *Inorg. Chem.*, 1984, **23**, 3398.
37 B. Chiari, O. Piovesana, T. Tarantelli and P. F. Zanazzi, *Inorg. Chem.*, 1982, **21**, 1396.
38 I. Shweky, A. Bino, D. P. Goldberg and S. J. Lippard, *Inorg. Chem.*, 1994, **33**, 5161.
39 S. J. Barclay, P. E. Riley and K. N. Raymond, *Inorg. Chem.*, 1984, **23**, 2005.
40 J. D. Walker and R. Poli, *Inorg. Chem.*, 1990, **29**, 756.
41 A. Elmali, Y. Elerman, I. Svoboda, H. Fuess, K. Griesar and W. Haase, *Z. Naturforsch.*, *Teil B*, 1994, **49**, 1239.
42 J. A. Bertrand, J. L. Breece and P. G. Eller, *Inorg. Chem.*, 1974, **13**, 125.
43 S. M. Gorun and S. J. Lippard, *Inorg. Chem.*, 1991, **30**, 1625.
44 H. Weihe and H. U. Güdel, *J. Am. Chem. Soc.*, 1997, **119**, 6539.
45 P. W. Anderson, *Solid State Phys.*, 1963, **14**, 25.
46 P. T. Kissinger and W. R. Heineman, in *Laboratory Techniques in Electroanalytical Chemistry*, ed. Marcel Dekker, Inc, New York, 1st edn., 1984, ch. 3, pp. 52–78.

Paper a908062g